J. Fluid Mech. (1998), *vol.* 369, *pp.* 151–173. Printed in the United Kingdom

Hydrodynamics of particles embedded in a flat surfactant layer overlying a subphase of finite depth

By HOWARD A. STONE[1,2] AND ARMAND AJDARI[2]

[1]Division of Engineering and Applied Sciences, Harvard University, Cambridge, MA 02138, USA

[2]Laboratoire de Physico-Chimie Théorique, URA CNRS 1382, ESPCI, 10 rue Vauquelin, 75231 Paris Cedex 05, France

(Received 4 August 1997 and in revised form 23 March 1998)

The motion of membrane-bound objects is important in many aspects of biology and physical chemistry. A hydrodynamic model for this Fconfiguration was proposed by Saffman & Delbrück (1975) and here it is extended to study the translation of a disk-shaped object in a viscous surface film overlying a fluid of finite depth H. A solution to the flow problem is obtained in the form of a system of dual integral equations that are solved numerically. Results for the friction coefficient of the object are given for a complete range of the two dimensionless parameters that describe the system: the ratio of the sublayer (η) to membrane (η_m) viscosities, $\Lambda = \eta R/\eta_m h$ (where R and h are the object radius and thickness of the surface film, respectively), and the sublayer thickness ratio, H/R. Scaling arguments are presented that predict the variation of the friction coefficient based upon a comparison of the different length scales that appear in the problem: the geometric length scales H and R, the naturally occurring length scale $\ell_m = \eta_m h/\eta$, and an intermediate length scale $\ell_H = (\eta_m h H/\eta)^{1/2}$. Eight distinct asymptotic regimes are identified based upon the different possible orderings of these length scales for each of the two limits $\Lambda \ll 1$ and $\Lambda \gg 1$. Moreover, the domains of validity of available approximations are established. Finally, some representative surface velocity fields are given and the implication of these results for the characterization of hydrodynamic interactions among membrane-bound proteins adjacent to a finite-depth sublayer is discussed briefly.

1. Introduction

The observed motion and diffusion of proteins, or other membrane-bound particles, in biological or artificial membranes are complicated frequently by the presence of nearby rigid boundaries. A starting point for the analysis and quantitative understanding of these systems is the hydrodynamic model for protein motion in bilayers presented by Saffman (1976; see also Saffman & Delbrück 1975). This model treats the translation and/or rotation of a thin disk in a thin viscous sheet overlying a liquid layer of infinite depth. The subphase underlying the viscous surface film has a significant, and in some cases, dominant effect on the motion and so cannot be neglected in analyses of the motion of a membrane-bound particle even in the limit that the subphase is much less viscous than the surface film. The topic of resistance from a subphase, as well as the effect of nearby boundaries, is also important for the characterization of supported membranes (e.g. Sackmann 1996), for estimating the

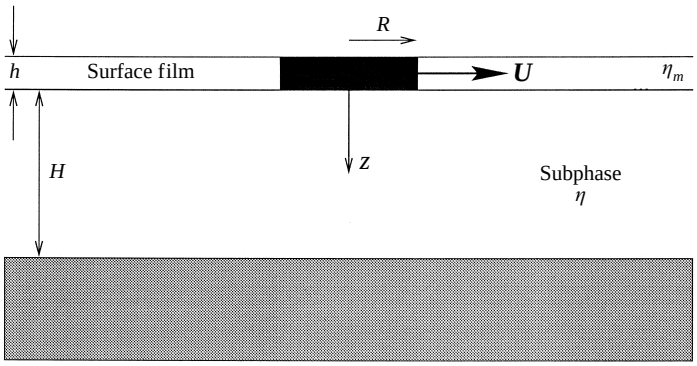

FIGURE 1. A hydrodynamic model of a membrane-bound object, modelled as a rigid cylinder, translating in a fluid film above a (Newtonian) subphase of finite depth.

influence of microscope slides and nearby substrates on laboratory measurements of lipid, protein and domain diffusion in membranes (Merkel, Sackmann & Evans 1989; H. M. McConnell, private communication), and for quantifying the reduced lateral diffusion of a protein in a bilayer which is itself surrounded by other bilayers (Peters & Cherry 1982). Here we generalize Saffman's analysis to account for the influence on particle translation of a nearby rigid plane boundary below the membrane.

There are several situations where particle motion in a surface film (e.g. a monolayer or bilayer) occurs. As mentioned, one example is the diffusion of proteins along a cell membrane. Also, it is known that phase separation, leading to the formation of finite-sized domains, occurs readily in surface monolayers consisting of multiple chemical components (McConnell 1991); the smaller of these domains, generally a few microns in radius, undergo Brownian motion while the larger domains are readily moved using an electric field. A hydrodynamic model for the translation of a membrane-bound protein or larger domain is sketched in figure 1. Typically, the amphiphilic membrane has a viscosity $\eta_m \approx 1$ P, the aqueous subphase has viscosity $\eta \approx 10^{-2}$ P, and h has molecular dimensions, say 30 Å. Proteins typically have molecular dimensions also, in which case $R \approx 30$ Å, while phase-separated domains characteristic of the liquid-expanded/liquid-condensed phase coexistence region have typical radii $R \approx 5$–100 μm (McConnell 1991). A dimensionless parameter Λ that characterizes the flow involves the ratio of viscosities of the surface layer and the subphase, $\Lambda = \eta R/\eta_m h$, and may take on a wide range of values, $10^{-3} < \Lambda < 10^3$. The principal hydrodynamic contribution of the research reported here is to allow for variable sublayer depths by considering configurations where the sublayer may be very deep, $H \gg R$, have intermediate depths, $H > R$, as well as accounting for a very thin subphase, $H \approx R$ for the protein diffusion applications or $H \ll R$ for the case of larger domains.

This 'particle-trapped-in-a-plane' geometry was first studied quantitatively by Saffman (1976) who presented an approximate solution for the force acting on a translating cylinder, which spans the width of a planar layer, and so is treated as a thin disk translating in the plane $z = 0$. The membrane and subphase are treated as continua and each is modelled as a constant-viscosity Newtonian fluid. The membrane is assumed to remain planar and viscous stresses exerted from the subphase are assumed to be transmitted uniformly across the thin surface film so that the membrane flow is two-dimensional.

Saffman presented an approximate analytical solution valid for $\Lambda = \eta R/\eta_m h \ll 1$.

The problem was later examined in detail by Hughes, Pailthorpe & White (1981) who developed an analytical solution for all Λ. A discussion of the application of these hydrodynamic analyses to the diffusion of protein molecules in lipid bilayers is given by Clegg & Vaz (1985); also Vaz *et al.* (1987) discuss the applicability of these models for the interpretation of experiments on the diffusion of lipid molecules in lipid bilayers. Recently, Bussell, Koch & Hammer (1992) and Bussell, Hammer & Koch (1994) extended Saffman's approximate solution in order to treat multiple particles trapped in a bilayer. A common feature of all of these theoretical analyses is that the sublayer is treated as infinitely deep and that the surface remains flat as a result of the amphiphilic character of the membrane molecules producing a significant resistance to surface distortion. A generalization of Saffman's solution approach was described by Stone & McConnell (1994) in a study of the dynamics of the shape instabilities of nearly circular lipid domains; the finite thickness of the sublayer fluid was also treated (Stone & McConnell 1995). In each of the above theoretical analyses of planar, horizontally unbounded surface layers it was demonstrated that there was no vertical component of velocity in the subphase so that the disk motion in the surface layer resulted in a laminar sublayer flow restricted to planes parallel to the surface. Here we will make this ansatz at the outset (§ 2) and at each step in our analysis it should be clear that the solution described below satisfies the governing equations and boundary conditions.

A valuable addition to the subject of protein diffusion in membranes was presented by Evans & Sackmann (1988) who extended the hydrodynamic model to treat translation and rotation of disk-shaped particles in membranes separated from a substrate by a very thin film. However, the general case of arbitrary-thickness sublayers has not been studied. The numerical results presented here demonstrate that the model proposed by Evans & Sackmann (1988) may be quite accurate even when the sublayer is not particularly thin, and scaling arguments, corroborated by examination of the numerical results presented in §§ 3 and 4, demonstrate that 'thin' essentially means $H < R\Lambda^{-1}$, at least for viscous membranes $\Lambda \ll 1$.

We first present in § 2.1 the basic hydrodynamic description for the motion coupling the surface film to the viscous subphase. The boundary value problem leads to dual integral equations whose solution is outlined in § 2.2. Several asymptotic formulae, valid either for $\Lambda \ll 1$ and deep sublayers, or for thin sublayers, are summarized in § 2.3. Numerical results for the dimensionless force as a function of Λ and H/R are given in § 3. In § 4 scaling arguments are presented for the two physical limits of most interest, $\Lambda \ll 1$ and $\Lambda \gg 1$, and the orders of magnitude of the force as a function of the sublayer depth H/R are deduced. The asymptotic formulae and the scaling arguments are compared with the numerical results in order to demonstrate the range of validity of the approximations. The structure of the surface velocity field is also shown. Finally, we close with a comment regarding the effect of a finite-depth sublayer on hydrodynamic interactions.

2. Problem formulation and solution

2.1. *Governing equations*

We first consider the form of the velocity field in the subphase for a particle translating at a specified velocity along the surface, then analyse motion in the surface film, and using both results determine the total force acting on the translating particle. The interface is assumed to remain flat over distances much larger than the particle

radius and so flow occurs bounded by two infinite horizontal boundaries (figure 1). We denote by $\boldsymbol{u} = (u_r, u_\theta, u_z)$ and p the subphase velocity and pressure fields, respectively, and use a cylindrical (r, θ, z) coordinate system with z directed into the subphase toward the rigid boundary. The Stokes and continuity equations apply in the subphase liquid, which is treated as incompressible:

$$-\nabla p + \eta \nabla^2 \boldsymbol{u} = \boldsymbol{0} \quad \text{and} \quad \nabla \cdot \boldsymbol{u} = 0. \tag{1}$$

Everywhere along the bottom boundary $z = H$ the no-slip condition, $\boldsymbol{u} = \boldsymbol{0}$, must be satisfied while in the plane $z = 0$ the disc-shaped particle translates with velocity $\boldsymbol{U}$. Assuming that $u_z \equiv 0$ everywhere (which may either be demonstrated explicitly or verified *a posteriori*), the hydrodynamic pressure field associated with this surface-driven Stokes flow is simply $p \equiv$ constant (e.g. Stone & McConnell 1994). The velocity field is thus confined to planes $z =$ constant and has the form

$$u_r(r, \theta, z) = U \cos\theta \int_0^\infty A(k) \sinh\left[k(H - z)\right] \left\{J_2(kr) + J_0(kr)\right\} \, \mathrm{d}k, \tag{2a}$$

$$u_\theta(r, \theta, z) = U \sin\theta \int_0^\infty A(k) \sinh\left[k(H - z)\right] \left\{J_2(kr) - J_0(kr)\right\} \, \mathrm{d}k, \tag{2b}$$

where $J_n(s)$ is the Bessel function of the first kind and $A(k)$ is a dimensionless function to be determined. We note that if the surface film is surrounded above and below by the same fluid and bounded at equal distances above and below by a rigid boundary, then, owing to the symmetry of the configuration, equations $(2a, b)$ may be applied for all z provided z is replaced by $|z|$; an obvious generalization can handle different fluids (e.g. Hughes *et al.* 1981) or different locations of the rigid boundaries.

The membrane velocity field $\boldsymbol{u}_m$ must conform to this same velocity representation and by no-slip must equal the sublayer velocity evaluated at $z = 0$, i.e. $\boldsymbol{u}_m(r, \theta) = \boldsymbol{u}(r, \theta, z = 0)$:

$$u_{mr}(r, \theta) = U \cos\theta \int_0^\infty A(k) \sinh(kH) \left[J_2(kr) + J_0(kr)\right] \, \mathrm{d}k, \tag{3a}$$

$$u_{m\theta}(r, \theta) = U \sin\theta \int_0^\infty A(k) \sinh(kH) \left[J_2(kr) - J_0(kr)\right] \, \mathrm{d}k. \tag{3b}$$

The membrane continuity equation $\nabla \cdot \boldsymbol{u}_m = 0$ is of course automatically satisfied.

The disk translates in the x–direction, $\boldsymbol{U} = U(\boldsymbol{e}_r \cos\theta - \boldsymbol{e}_\theta \sin\theta)$, so that for $r < R$ the unknown function $A(k)$ satisfies

$$1 = \int_0^\infty A(k) \sinh(kH) \left[J_2(kr) + J_0(kr)\right] \, \mathrm{d}k \quad \text{for} \quad r < R, \tag{4a}$$

$$-1 = \int_0^\infty A(k) \sinh(kH) \left[J_2(kr) - J_0(kr)\right] \, \mathrm{d}k \quad \text{for} \quad r < R. \tag{4b}$$

As $J_2(s) + J_0(s) = 2J_1(s)/s$, it is convenient to write $(4a)$ as

$$\frac{r}{2} = \int_0^\infty A(k) k^{-1} \sinh(kH) J_1(kr) \mathrm{d}k \quad \text{for} \quad r < R. \tag{5}$$

Differentiating (5) with respect to r yields $(4b)$, and below we find it convenient to work with (5).

For $r > R$ we must consider the equation of motion for the monolayer or bilayer film, which is assumed to be Newtonian (there are recent observations of non-Newtonian effects in the flow of some surface films, e.g. D. K. Schwartz, G. G. Fuller,

private communications). The film fluid is assumed to remain planar so that the surface layer hydrodynamics are effectively two-dimensional. In this case a Stokes-like equation is appropriate with an additional body force $\boldsymbol{f}$ exerted on the surface layer by viscous stresses arising from motion in the underlying liquid (Saffman 1976). Further, here we suppose that air or another fluid of viscosity much less than that of the subphase overlays the system, though we note that the steps in the analysis can be generalized to account for dynamical influences in an upper phase. The body force per unit volume of the surface layer may then be written

$$\boldsymbol{f} = \frac{1}{h}\boldsymbol{e}_z \cdot \boldsymbol{\sigma}|_{z=0}, \tag{6}$$

where $\boldsymbol{\sigma}$ is the stress tensor for the subphase flow, $\boldsymbol{\sigma} = -p\boldsymbol{I} + \eta\left(\nabla\boldsymbol{u} + (\nabla\boldsymbol{u})^T\right)$. Thus, the membrane motion satisfies

$$-\nabla p_m + \eta_m \nabla^2 \boldsymbol{u}_m + \boldsymbol{f} = \boldsymbol{0} \quad \text{and} \quad \nabla \cdot \boldsymbol{u}_m = 0, \tag{7}$$

where η_m is the shear viscosity of the membrane fluid (note that the commonly used 'surface shear viscosity' is $\eta_m h$ and has units of viscosity $\times$ length). Taking the curl of equation (7) to eliminate the pressure and substituting the given expressions for the velocity field we eventually arrive at a surface flow condition in the form

$$\int_0^\infty A(k)k^2 \left[k\sinh(kH) + \frac{\eta}{\eta_m h}\cosh(kH)\right] J_1(kr)\,\mathrm{d}k = 0 \quad \text{for} \quad r > R. \tag{8}$$

At this point we have two equations, (5) and (8), which serve to define the function $A(k)$. To generalize these results to the case of a layer midway between rigid plane boundaries with the same fluid on both sides, η in equation (8) is replaced by 2η. Now, after scaling all lengths in (5) and (8) by R, and letting $s = kR$, $\bar{r} = r/R$, and $A(k) = RB(s)$, we obtain the dual integral equations

$$\int_0^\infty B(s)s^{-1}\sinh(sH/R)J_1(s\bar{r})\,\mathrm{d}s = \frac{\bar{r}}{2} \quad \text{for} \quad \bar{r} < 1, \tag{9a}$$

$$\int_0^\infty B(s)s^2\cosh(sH/R)\left[s\tanh(sH/R) + \Lambda\right] J_1(s\bar{r})\,\mathrm{d}s = 0 \quad \text{for} \quad \bar{r} > 1, \tag{9b}$$

where the dimensionless parameter Λ represents the effective viscosity contrast between the surface film and the subphase fluid,

$$\Lambda = \frac{\eta R}{\eta_m h}. \tag{10}$$

These dual integral equations, (9*a*) and (9*b*), with Bessel function kernels have the form considered by Tranter (1966) and in the next subsection we outline how to solve these equations numerically using a series representation for $B(s)$, which we shall refer to as 'Tranter's method'. Once $B(s)$, or equivalently $A(k)$, is known the detailed flow field can be obtained from (2) and (3), and can be used to determine the membrane pressure field p_m and the total force acting on the translating disk.

It is straightforward, though tedious, to show that the membrane pressure field is (the often discussed and measured 'surface pressure' corresponds to hp_m)

$$p_m(r,\theta) = \frac{\eta_m U}{R}\cos\theta \int_0^\infty A(k)kr\cosh(kH)\left[kR\tanh(kH) + \Lambda\right](J_2(kr) - J_0(kr))\,\mathrm{d}k. \tag{11}$$

As mentioned earlier, we make the common assumption that the films remains flat, even in the presence of variations of p_m, owing to molecular scale resistance to surface distortion (amphiphilic molecules resist such configurational changes). Also, the total force $\boldsymbol{F}$ acting on the translating disc, the force being exerted both by the membrane fluid over the perimeter $2\pi Rh$ and the subphase fluid over the area πR^2, may be shown to be

$$\boldsymbol{F} = -\frac{2\pi\eta R\boldsymbol{U}}{\Lambda}\int_0^\infty B(s)s\cosh(sH/R)\left[s\tanh(sH/R)+\Lambda\right]J_2(s)\,\mathrm{d}s. \tag{12}$$

The velocity field and torque for a disk-shaped particle rotating in a surface film bounded below by a sublayer of finite depth can also be determined. The details are similar to those given above and, since this problem is of less interest, the details are not presented here. For both the translation and rotation problems, the determination of the velocity field and corresponding force and torque depends on two parameters, Λ and H/R.

2.2. *Solution of the dual integral equations*

Saffman (1976) and Hughes *et al.* (1981) studied the deep subphase limit $H/R \to \infty$ and our equations reduce to theirs in this limit. Saffman presented an approximate analytical solution for the force acting on the disc in the limit $\Lambda \ll 1$ (equation (18) below). Hughes *et al.* applied to the dual integral equations an analytical procedure using Erdélyi–Kober operators (e.g. Sneddon 1966) to develop a solution valid for all Λ and in particular derived an approximate expression for the force valid for $\Lambda < 0.6$ (equation (19)). We were not successful in applying the Erdélyi–Kober operator technique to the set of dual integral equations developed in § 2.1 owing to the more complicated form of the integral kernels. Instead we have developed a direct numerical approach to solve for $A(k)$ and so determine the flow field and force.

Tranter's method (Tranter 1966) consists of representing the unknown function in terms of a series of Bessel functions. Hence, we take

$$B(s)s^2\cosh(sH/R)\left[s\tanh(sH/R)+\Lambda\right] = s^{1-\beta}\sum_{m=0}^{\infty} a_m J_{2m+1+\beta}(s), \tag{13}$$

where the $\{a_m\}$ are constants to be determined and β (> 0) is a parameter which controls the convergence of integrals and for which there is a 'best' value that captures the singular nature of the mathematical problem in the neighbourhood of the disk edge (e.g. Ungarish & Vedensky 1995; Tanzosh & Stone 1995). The representation (13) automatically satisfies equation (9*b*); e.g. see Gradshteyn & Ryzhik (1965, equation 6.574.1). Substituting (13) into (9*a*) and following a series of steps first outlined by Tranter to eliminate the dependence on $\bar{r}$ (analogous to an orthogonality relationship), we find that the $\{a_m\}$ satisfy the (infinite) linear system of equations

$$\sum_{m=0}^{\infty} a_m \int_0^\infty \frac{s^{-2-2\beta}\tanh(sH/R)}{\left[s\tanh(sH/R)+\Lambda\right]} J_{2m+1+\beta}(s)J_{2n+1+\beta}(s)\,\mathrm{d}s = \frac{\delta_{0n}}{2^{\beta+1}\Gamma(\beta+2)}, \quad n = 0, 1, \ldots, \tag{14}$$

where $\Gamma(s)$ is the Gamma function. It is now straightforward to determine the $\{a_m\}$ by truncating (14) to a finite system of N equations, evaluating the infinite integrals involving products of Bessel functions using the numerical routines described by Lucas (1995), and inverting the resulting matrix. We have performed calculations for different values of β, which of course changes the specific values of the $\{a_m\}$ but

not any of the physical results. Choices of β closer to zero give more robust results since the integrals converge more quickly and the resulting matrix problem is easier to solve. Typically we choose $N = 8 - 20$ and use larger N for smaller H/R.

Substituting (13) into (12), and using the identity (Gradshteyn & Ryzhik 1965, equation 6.574.2)

$$\int_0^\infty s^{-\beta} J_2(s) J_{2m+1+\beta}(s)\,\mathrm{d}s = \frac{\delta_{0m}}{2^\beta \Gamma(2+\beta)}, \tag{15}$$

one can show that the total hydrodynamic force acting on the cylinder is given by

$$\boldsymbol{F} = -\frac{2\pi\eta R \boldsymbol{U} a_0}{\Lambda 2^\beta \Gamma(2+\beta)}, \tag{16}$$

which conveniently only involves a_0. The drag coefficient is then defined as $\zeta_{\mathrm{Stokes}} \equiv |\boldsymbol{F}|/|\boldsymbol{U}|$.

Once the force acting on a steadily translating disk is calculated the translational diffusion coefficient follows from the Stokes–Einstein equation,

$$D_T = \frac{k_B T}{|\boldsymbol{F}|/|\boldsymbol{U}|} = \frac{k_B T}{\zeta_{\mathrm{Stokes}}}, \tag{17}$$

where k_B is Boltzmann's constant and T is the absolute temperature. Hence, we can evaluate the diffusion coefficient for any values of the dimensionless sublayer depth H/R and the viscosity ratio between the surface film and sublayer fluids as measured by Λ. We will report in § 3 dimensionless values of ζ_{Stokes} as a function of Λ and H/R.

2.3. *Existing approximations for $\Lambda = \eta R/\eta_m h \ll 1$ or thin sublayers*

In Saffman's original analysis, an approximate expression was derived for the force exerted by the fluid on the particle in the limit $\Lambda \ll 1$ and $H/R \to \infty$. In our notation, and accounting for resistance from a fluid below the membrane only, Saffman's force equation is

$$\boldsymbol{F}_{\mathrm{Saffman}} = -\frac{4\pi\eta R \boldsymbol{U}}{\Lambda\left[\ln(2/\Lambda) - \gamma\right]} \quad (\Lambda \ll 1), \tag{18}$$

where $\gamma \approx 0.5772$ is Euler's constant. Hughes *et al.* (1981) developed an improved asymptotic expansion for the force as a function of Λ:

$$\boldsymbol{F}_{\mathrm{Hughes}} = -\frac{4\pi\eta R \boldsymbol{U}}{\Lambda\left[\ln(2/\Lambda) - \gamma + (4/\pi)^{1/2}\Lambda - \frac{1}{2}\Lambda^2 \ln(2/\Lambda)\right]} \quad (\Lambda < 1). \tag{19}$$

Hughes *et al.* compared this equation with their numerical results and found excellent agreement for $\Lambda < 0.6$.

More recently Evans & Sackmann (1988) presented a simple model for accounting for the additional resistance produced by a rigid planar boundary in the limit that the sublayer is thin (see also Brochard, Joanny & Andelman 1987). Evans & Sackmann introduced a friction parameter b_s for the drag on the membrane from the substrate. With the sublayer flow approximated as a simple shear flow, then $\boldsymbol{f} = -\eta \boldsymbol{u}_m/H$ (see equations (7) and (22) in § 4) and $b_s = \eta/H$, so the dimensionless parameter ϵ used by Evans & Sackmann is in our notation

$$\epsilon^2 = \Lambda \frac{R}{H} \quad \text{(Evans–Sackmann)}. \tag{20}$$

These authors also used a friction coefficient b_p for the drag on the particle directly from the substrate and for the idealized case considered here $b_p = b_s$. The force on the

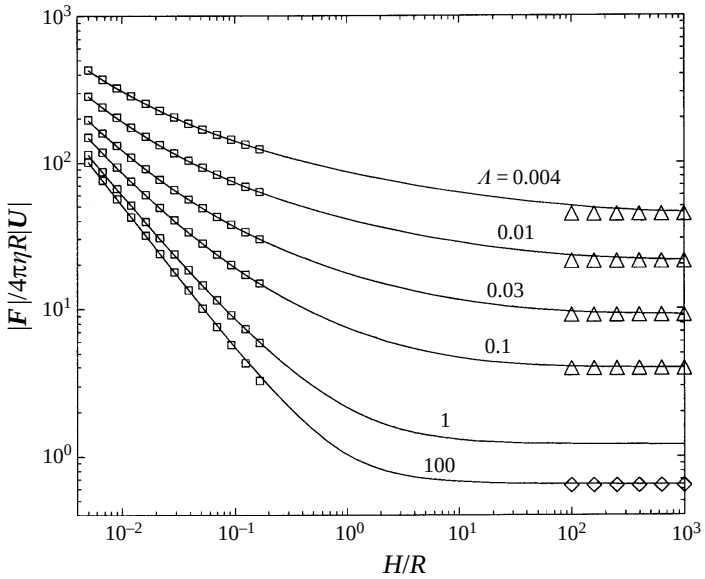

FIGURE 2. Variation of the dimensionless drag coefficient $|\boldsymbol{F}|/4\pi\eta R|\boldsymbol{U}|$ as a function of H/R; $\Lambda = 0.004, 0.01, 0.03, 0.1, 1$ and 100. Comparison is provided with three known limits: (i) the triangles to the far right indicate the infinite-subphase limit, $H \to \infty$, calculated using the equation of Hughes *et al.* (1981) for $\Lambda < 0.6$; (ii) the diamonds to the far right correspond to the infinite-subphase limit for the case $\Lambda \to \infty$ where the dimensionless drag coefficient equals $2/\pi$ (see Appendix A); (iii) the square symbols shown to the left are the predictions of the Evans–Sackmann formula (equation (21)), which was developed for very thin sublayers.

translating object was then calculated for membrane-trapped particle motion above thin sublayers to be

$$\boldsymbol{F}_{\mathrm{E-S}} = -\frac{4\pi\eta R\boldsymbol{U}}{\Lambda}\left[\frac{1}{2}\epsilon^2 + \frac{\epsilon K_1(\epsilon)}{K_0(\epsilon)}\right], \tag{21}$$

where the $K_n(s)$ are modified Bessel functions.

We shall use the numerical solution presented in § 2.2 to illustrate in §§ 3 and 4 the validity of these different approximations as Λ and H/R are varied. In addition, in § 4 (equation (23)), a drag expression for a finite depth subphase, analogous to (18), is introduced.

3. Numerical results: force as a function of Λ and H/R

The numerical results are independent of the specific value of β and for the calculations presented below we choose $\beta = 1/8$. We have verified that as the number of terms N in the series solution (13) is increased there is convergence for the values of the coefficients $\{a_m\}$. We showed in § 2.2 that the determination of the force acting on the translating disc only requires knowledge of a_0 (equation (16)). Using ten terms in the series solution, we obtain about 1% accuracy in the values of a_0 though, if details of the velocity field are desired, more terms in the expansion are typically required.

In figure 2 we illustrate the variation of the dimensionless force, or drag coefficient, $|\boldsymbol{F}|/4\pi\eta R|\boldsymbol{U}|$ (this choice for non-dimensionalization of the force is common), as a function of the dimensionless sublayer depth H/R for $5 \times 10^{-3} \leqslant H/R \leqslant 10^3$.

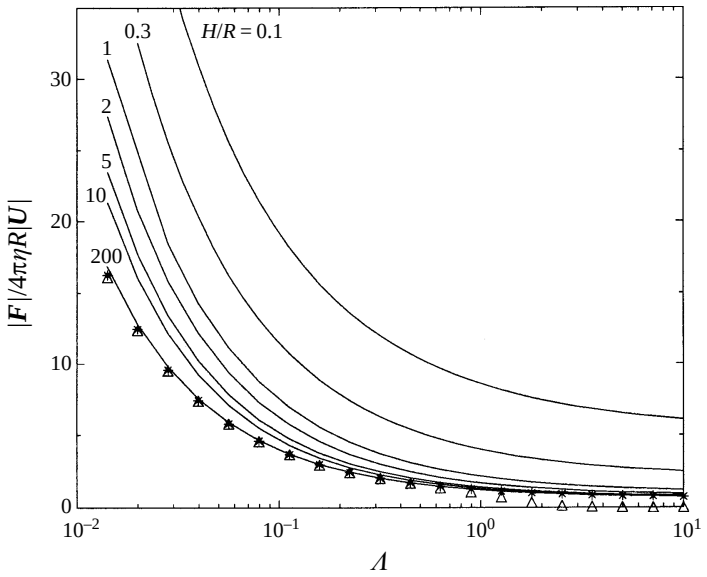

FIGURE 3. Variation of the dimensionless drag coefficient on a steadily translating disk as a function of Λ and H/R. The triangles correspond to the approximate formula derived by Hughes *et al.* (equation (19) above). The stars indicate our numerical results for $H/R = 10^3$ and are displayed here simply to illustrate that $H/R = 200$ is nearly 'infinite' for the values of Λ shown.

Although for the case of protein diffusion in bilayers this hydrodynamic model only seems reasonable provided $H/R \geqslant 1$, the translation of larger membrane-trapped particles can correspond to $H/R < 1$, and such values are presented for completeness. Results for six values of Λ are shown in figure 2 which span the most likely values of the viscosity contrast to be expected for a wide range of situations. The numerical results are shown by the solid curves and three asymptotic results are presented: (i) triangles to the far right indicate the infinite-subphase limit calculated using the asymptotic formula developed by Hughes *et al.*, equation (19), (ii) diamonds to the far right correspond to the infinite subphase limit with $\Lambda \to \infty$ for which there is the analytical result $F/4\pi\eta RU = 2/\pi$ (see Appendix A), (iii) the square symbols are the predictions of the Evans–Sackmann formula (equation (21)) for thin sublayers. These asymptotic approximations are included to emphasize the accuracy of the numerical calculations. Detailed comparisons with the asymptotic formulae summarized in § 2.3 are presented in § 4. For now we observe that the numerical results are in excellent agreement with available approximations for $H/R \ll 1$ and $H/R \gg 1$. Qualitatively, for a fixed value of H/R and sublayer viscosity η, lower values of Λ correspond to more viscous surface films and higher drag coefficients.

In figure 3 we show the variation of the dimensionless drag coefficient $\zeta_{Stokes}/4\pi\eta R$ as a function of Λ for seven different values of H/R. The triangles correspond to the asymptotic approximation (19), valid for small Λ and an infinitely deep subphase, $H/R \to \infty$, and the stars are our numerical results for $H/R = 10^3$. The agreement is excellent between the asymptotic approximation and the numerical results, and as indicated by Hughes *et al.* their asymptotic formula (19) is very accurate for $\Lambda < 0.6$. Similarly, we have verified that our results for $\Lambda > 1$ are in excellent agreement with the numerical values for the force reported by Hughes *et al.* In figure 3 we observe the significant influence of the rigid lower boundary as H/R decreases. For $\Lambda > 10$ and

$H/R > 1$, however, there is only a small variation of the force as the sublayer depth is varied. The dependence of the corresponding diffusion coefficient on the depth of the sublayer then follows by combining the results shown in figure 3 with equation (17). Thus, one can expect that measured diffusion coefficients for membrane-bound proteins ($\Lambda \ll 1$) above a sublayer with $H/R \approx 1$ are about half their value above an unbounded subphase provided no other physical influences are hindering or otherwise affecting the diffusion.

4. Dependence of the force on Λ and H/R

In order to explore completely the dependence of the friction coefficient on Λ and H/R it is useful to provide a physical description of the typical forces to be expected when an inclusion translates parallel to the membrane surface and so is resisted by viscous stresses from both the membrane and the sublayer. A convenient way to organize the presentation is in terms of the relevant geometrical and dynamical length scales. There are two geometric length scales, R and H (we are viewing the dynamics on scales large compared to h, so do not include h as an independent length scale). In addition, for motions far from boundaries there is a naturally occurring 'material' length scale, $\ell_m = \eta_m h/\eta$, which, referring to equation (7), characterizes the distance at which viscous forces per unit volume due to membrane flow $O(\eta_m U/\ell_m^2)$ are comparable to the viscous forces per unit volume exerted on the membrane from the sublayer $O(\eta U/h\ell_m)$. Note that $R/\ell_m = \Lambda$. We will see below that when the effect of the nearby solid boundary is significant, there is an additional relevant length scale $\ell_H = (\ell_m H)^{1/2}$, which is therefore intermediate between H and ℓ_m.

There are two obvious limits, largely set by material properties, to consider: $\Lambda^{-1} = \ell_m/R \gg 1$ and $\Lambda = R/\ell_m \gg 1$. In order to identify the important physical balances we first consider an *infinite* subphase, which requires $R, \ell_m \ll H$. When $\ell_m < R$, the flows in the monolayer and the sublayer are disturbed on a length scale R and the drag force on the translating membrane-bound object is expected to be $O(\eta RU)$, a result which is consistent with the largest viscous dissipation occurring throughout a volume $O(R^3)$. On the other hand, for $\ell_m \gg R$, representative of protein motion in surface films much more viscous than the surrounding fluid, there are long-range (compared to R) surface flows generated as elegantly analysed by Saffman (1976). The local monolayer flow near the translating object is that for a cylinder translating in a purely viscous fluid (Stokes flow) and this two-dimensional flow involves a logarithmic variation of velocity disturbances (Stokes's paradox). At large distances the particle acts as a point force, and the viscous resistance from the surrounding fluid phase is responsible for eliminating the divergence, with the cut-off occurring at a distance $O(\ell_m)$. In this case, the force on the object is dominated by gradients in the monolayer, and typical velocity variations in the neighbourhood of the particle occur on a length scale $R\ln(\ell_m/R)$ (see Appendix B). The force follows from the product of the surface shear stress $O(\eta_m U/R\ln(\ell_m/R))$ and the surface area $2\pi Rh$. Thus, for infinite depth sublayers the force is expected to be $O(\eta_m Uh/\ln(\ell_m/R)) = O(\eta RU/\Lambda\ln(\Lambda^{-1}))$, which is in agreement with the form of equations (18) and (19). For the small-Λ limit, a discussion of the local flow and the dependence of the velocity gradient, and so the force, on the logarithm of Λ is given in Appendix B.

Of course, in any real experiment, there are other physical effects that can act to eliminate the logarithmic divergence. Such possibilities include the effect of boundaries at large radial distances, inertial effects in the monolayer, which enter at a typical

Ordering of length scales	Dimensionless characterization	$\dfrac{\text{Force}}{\eta R U}$
$H \ll \ell_H \ll \ell_m \ll R$	$H/R \ll \Lambda^{-1} \ll 1$	$O(R/H)$
$\ell_m \ll \ell_H \ll H \ll R$	$\Lambda^{-1} \ll H/R \ll 1$	$O(R/H)$
$\ell_m \ll \ell_H \ll R \ll H$	$1 \ll H/R \ll \Lambda$	$O(1)$
$\ell_m \ll R \ll \ell_H \ll H$	$1 \ll \Lambda \ll H/R$	$O(1)$

TABLE 1. Summary of different estimates for the resistance to motion of a membrane-trapped object in the limit $\Lambda = \eta R/\eta_m h \gg 1$. Moving in the table from top to bottom corresponds to progressively increasing the thickness of the sublayer. $\ell_H = (\eta_m h H/\eta)^{1/2}$.

distance $O(R/\mathscr{R}_m)$, where $\mathscr{R}_m = RU/\nu_m \ll 1$ (ν_m is the kinematic viscosity of the surface film) is the monolayer Reynolds number for the particle motion (Saffman & Delbrück 1975), and a finite concentration of membrane-fixed particles (Dodd *et al.* 1995). The effect of a finite-depth subphase can also be important as we now detail.

In the presence of a finite-depth subphase, there are several additional possibilities for the magnitude of the resistance to translation. In particular, 'thin sublayers' were modelled by Evans & Sackmann (1988), though they did not specifically characterize the regime of validity of their analysis. For thin films the sublayer was assumed to undergo a simple shear flow $\boldsymbol{u} = (H - z)\boldsymbol{u}_m/H$, and so the equations of motion for the film are

$$\eta_m \nabla^2 \boldsymbol{u}_m - \nabla p_m - \frac{\eta \boldsymbol{u}_m}{Hh} = 0 \quad \text{and} \quad \nabla \cdot \boldsymbol{u}_m = 0. \tag{22a,b}$$

This form of the momentum equation is commonly referred to as the Brinkman equation. An exact solution is possible for the two-dimensional translation (or rotation) of a disc and the associated force is given in § 2.3. We note that a long-range motion in the surface film is expected when $\ell_m > R$, but now the subphase stresses arise from the shear flow in the thin film (exerting forces per unit volume $\eta U/hH$); the cut-off distance is therefore $\ell_H = (\eta_m h H/\eta)^{1/2}$ rather than ℓ_m, as can be seen by comparing the first and third terms in (22*a*).

There are thus, in general, three length scales to consider, R, H, and ℓ_m, as well as the intermediate length scale ℓ_H, and so there are eight possible dynamical limits depending on the relative sizes of these length scales. We shall discuss these limits by considering a given physical system ($\Lambda = R/\ell_m$ fixed) and imagine varying the sublayer from thin to thick. A summary of the different regimes is given in tables 1 and 2, and the regimes are also classified according to the relative magnitudes of the two dimensionless parameters, Λ and H/R. We will see below that the different regimes can be identified in the numerical results. Hence, these different physical estimates provide a convenient way to organize an understanding of the resistance to motion of membrane-trapped objects.

4.1. $\Lambda \gg 1$

Let us first consider $\Lambda = R/\ell_m \gg 1$. The different possibilities as the film thickness is varied are summarized in table 1, where the force for translation, normalized relative to $\eta R U$, is also given. For thin films, which means $H \ll \ell_m$, it is easy to see that a simple shear flow in the sublayer contributes a direct drag force $\pi R^2 \times \eta U/H$ on the particle's lower surface. It is also true, although on first examination this may appear surprising, that the incompressible monolayer flow makes a contribution of equal

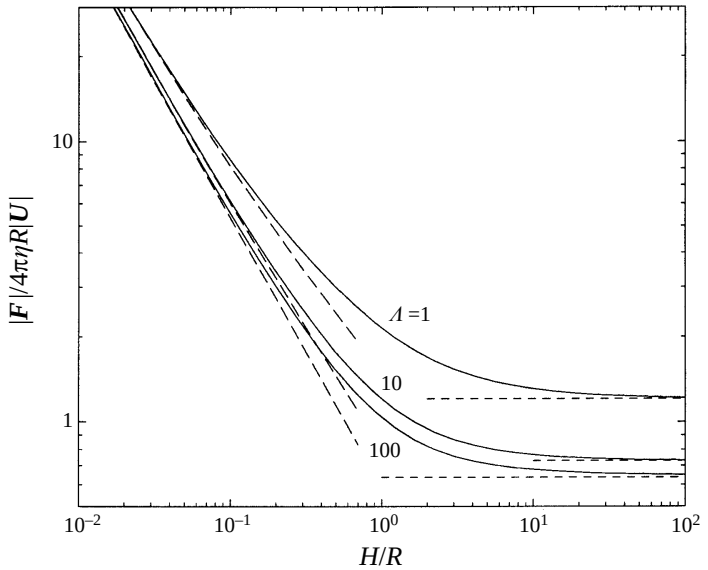

FIGURE 4. Force as a function of H/R for $\Lambda \geqslant 1$. The solid curves are calculated by solving the dual integral equations. The short-dashed lines on the right indicate the infinite-subphase limit, $H/R \gg 1$ (calculated numerically) and the long-dashed curves are calculated from equation (21) in the limit $\epsilon \gg 1$, i.e. $F/4\pi\eta RU = (R/H)(\frac{1}{2} + (H/R\Lambda)^{1/2})$.

Ordering of length scales	Dimensionless characterization	$\dfrac{\text{Force}}{\eta RU}$
$H \ll \ell_H \ll R \ll \ell_m$	$H/R \ll \Lambda \ll 1$	$O(R/H)$
$H \ll R \ll \ell_H \ll \ell_m$	$\Lambda \ll H/R \ll 1$	$O\left(\dfrac{1}{\Lambda \ln((H/R)\Lambda^{-1})}\right)$
$R \ll H \ll \ell_H \ll \ell_m$	$1 \ll H/R \ll \Lambda^{-1}$	$O\left(\dfrac{1}{\Lambda \ln((H/R)\Lambda^{-1})}\right)$
$R \ll \ell_m \ll \ell_H \ll H$	$1 \ll \Lambda^{-1} \ll H/R$	$O\left(\dfrac{1}{\Lambda \ln(\Lambda^{-1})}\right)$

TABLE 2. Summary of different estimates for the resistance to motion of a membrane-trapped object in the limit $\Lambda = \eta R/\eta_m h \ll 1$. The intermediate length scale $\ell_H = (\eta_m hH/\eta)^{1/2}$ plays an important role in determining the variation in the force as the sublayer thickness varies. Moving in the table from top to bottom corresponds to progressively increasing the thickness of the sublayer.

magnitude (and, in fact, equal value). Indeed, for a finite surface-film viscosity, no matter how small, the translation of the membrane-bound object generates motion in the film and sublayer on the scale R and, as a consequence of drag from the substrate, the motion is accompanied by a monolayer pressure drop $O(\eta RU/hH)$, which, acting over the particle circumference $2\pi Rh$, contributes a force $O(\eta R^2 U/H)$. In fact, expanding the thin-sublayer result of Evans & Sackmann, (21), for the large-Λ, thin-sublayer limit, i.e. $\epsilon \gg 1$, yields $F/4\pi\eta RU \approx (R/H)(\frac{1}{2} + (H/R\Lambda)^{1/2})$.

As H increases, it first becomes bigger than the small length ℓ_m, but as it remains smaller than R the force remains $O(\eta R^2 U/H)$. Increasing H further leads to the subphase becoming thicker than the particle scale R, at which point the diminished

viscous stresses lead to a force $O(\eta U/R \times \pi R^2) = O(\eta RU)$, and the drag becomes independent of H.

In figure 4 we present the dimensionless drag force for $\Lambda \geqslant 1$ and $10^{-2} \leqslant H/R \leqslant 10^2$. The numerical results (solid curves) are compared with the thin layer prediction $F/4\pi\eta RU \approx (R/H)(\frac{1}{2} + (H/R\Lambda)^{1/2})$ (long-dashed curves) and the infinite-sublayer limits (horizontal dashed lines, calculated numerically by taking $H/R = 10^3$) are shown also. There is very good agreement between the thin-layer approximation and the numerical results for $H/R < 0.2$. The two distinct possibilities for the magnitude of the force ($H/R < 1, H/R > 1$) described in the previous two paragraphs provide a good way to estimate the force for all H/R provided $\Lambda > O(1)$. The crossover between the two force estimates occurs at $H/R \approx 1$.

4.2. $\Lambda \ll 1$

The more varied, and so dynamically more interesting, case is that of a very thin viscous membrane $\Lambda = R/\ell_m \ll 1$, summarized in table 2. If the layer is very thin, with $H \ll \ell_H \ll R$, then the dominant resistance comes from the shear flow below the particle, and, as mentioned above, from the pressure drop in the incompressible monolayer flow due to overcoming drag from the substrate, and so the force is expected to be $O(\eta R^2 U/H)$.

On the other hand, as the sublayer is made deeper, the dominant contribution to the force comes from monolayer velocity gradients (i.e. shear stresses) that occur over a long distance (greater than R). The logarithmic divergence of the velocity disturbances must be cut off by sublayer motions and the cut-off length scale is the smallest of ℓ_H and ℓ_m. For example, after the thin-film limit, an increase in H may be interpreted as ℓ_H lying between R and ℓ_m. Thus, although the flow near the particle corresponds closely to that around a cylinder, beyond a distance ℓ_H the flow resembles the three-dimensional motion due to a point force in the film above the subphase. In the neighbourhood of the particle the velocity gradients are $O(U/R \ln(\ell_H/R))$ and the corresponding force is $F = O(\eta UR/\Lambda \ln((H/R)\Lambda^{-1}))$ and this contribution is larger than that from the sublayer due to the simple shear flow below the particle. Further increases in H move the flow out of the thin film limit, i.e. $H/R \gg 1$, but the force maintains the order of magnitude just obtained. Finally, increasing H so much that ℓ_H increases beyond ℓ_m, corresponds to the deep-subphase limit studied by Saffman for which $F = O(\eta UR/\Lambda \ln(\Lambda^{-1}))$. Therefore, we see that the boundary influence is expected to be important for $\ell_H < \ell_m$ or $H < R\Lambda^{-1}$.

A detailed analysis of this intermediate limit is possible, following the approach utilized by Saffman (1976), and this calculation is given in Appendix B. In particular for $R, H \ll \ell_m$, we find

$$\boldsymbol{F}_{\text{finite depth}} = -\frac{4\pi\eta R\boldsymbol{U}}{\Lambda\left[\ln(\Lambda R/4H)^{-1/2} - \gamma\right]}. \tag{23}$$

In figure 5 we focus on the small-Λ limit. The numerical results are shown as solid curves, the approximation for intermediate depths, equation (23), is shown as dot-dashed curves, and the predictions of the Saffman formula are shown at the far right with a star. For thin layers we have also compared the results with a three-term expansion of the Evans–Sackmann formula (21), i.e. $\epsilon \gg 1$ and $F/4\pi\eta RU \approx R/H(\frac{1}{2} + (H/R\Lambda)^{1/2} + H/2R\Lambda)$. Each of these simple approximations appears useful for a range of H/R, indicating the utility of the physical arguments given here, and the three approximations together allow a simple reconstruction of the entire curve for the dependence of the drag coefficient.

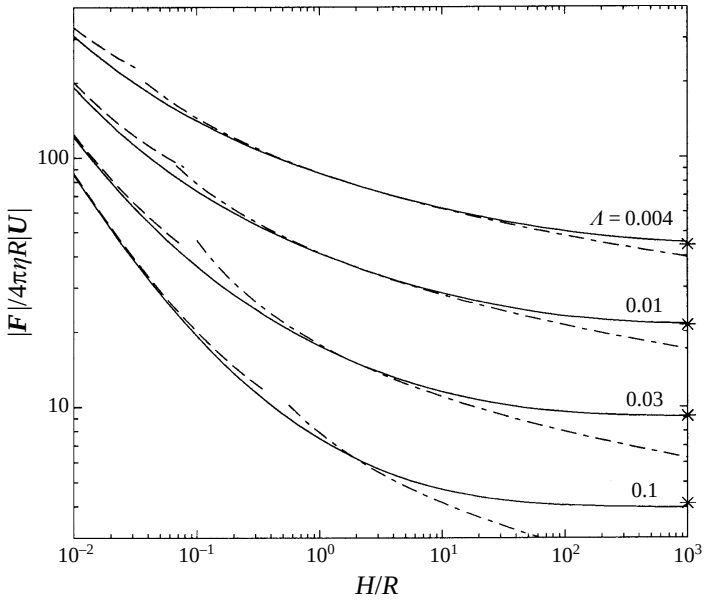

FIGURE 5. Force as a function of H/R for $\Lambda \ll 1$; solid curves are the numerical results calculated by solving the integral equations. The predictions of the Saffman formula for the infinite-subphase limit, $H/R \gg 1$, are shown as $*$, the long-dashed curves are the predictions of the Evans–Sackmann formula expanded to three terms, $F/4\pi\eta RU = (R/H)(\frac{1}{2} + (H/R\Lambda)^{1/2} + H/2R\Lambda)$ and the dot-dashed curve is the intermediate approximation, equation (23), for which the nearby rigid boundary provides a cut-off length scale of the logarithmically varying velocity disturbances of the two-dimensional surface flow near the translating disk.

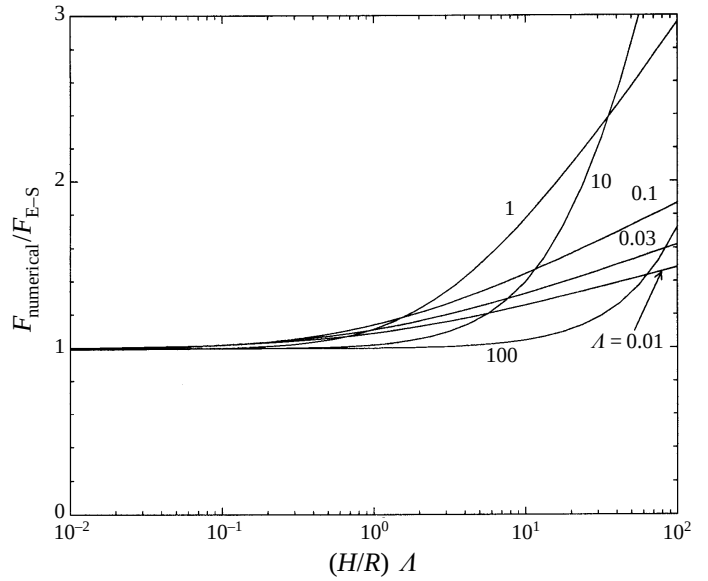

FIGURE 6. Force on the translating membrane-bound object for different Λ where the force is normalized using the value calculated according to the Evans–Sackmann 'thin-layer' formula, equation (21). The results demonstrate the range of validity of the Evans–Sackmann 'thin-film' formula and show the emergence of the effect of the 'deep' sublayer for $H/\ell_m > 1$ for $\Lambda < 1$.

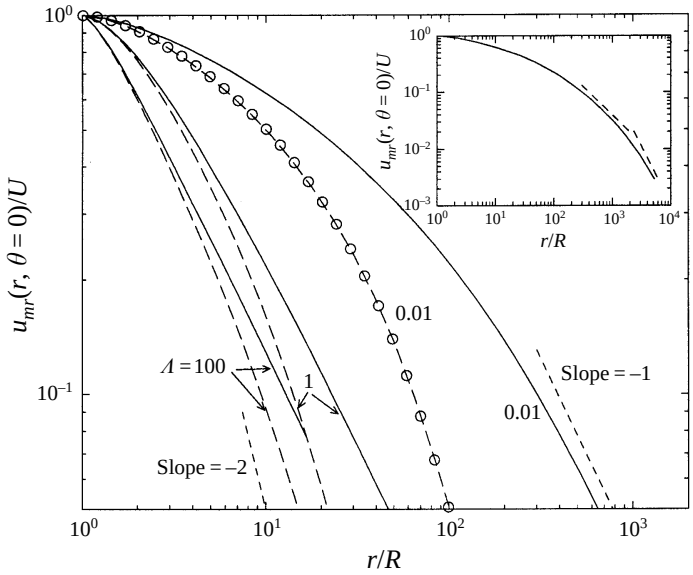

FIGURE 7. Radial velocity field as a function of the dimensionless radial distance for two sublayer depths, $H/R = 2000$ (solid curves) and $H/R = 10$ (long-dashed curves), and three values of $\Lambda = 100, 1$ and 0.01; short-dashed lines indicate slopes of -1 and -2. Also shown on the $\Lambda = 0.01$, $H/R = 10$ plot are circles corresponding to the velocity field calculated by Evans & Sackmann (1988) based on the thin-film model. The inset illustrates $\Lambda = 0.01$ and $H/R = 2000$ which has been calculated to large enough r that the transition from a decay rate r^{-1} to r^{-2} is observed (the dashed curves have slope -1 and -2).

4.3. *Domain of validity of the Evans–Sackmann approximation*

The crossover indicated above where the effect of the solid boundary is expected to be significant is studied in figure 6 by plotting the drag force, normalized by the complete Evans–Sackmann formula, as a function of $(H/R)\Lambda$. In effect, this graph demonstrates the utility of the Evans–Sackmann formula (21). We thus see that the Evans–Sackmann drag formula provides an excellent approximation for $H/R < \Lambda^{-1}$ for $\Lambda < 1$. In other words, the 'thin-layer approximation' is useful for $H < \ell_m$, or typically $H/R \lesssim 100$, and holds for not so thin sublayers. Hence, the complete Evans–Sackmann formula correctly describes the first three regimes indicated in table 2 (and an expansion of the Bessel functions in equation (21) yields the functional forms shown). In figure 6 we have also displayed results for $\Lambda = 10$ and 100. Overall, we observe that the Evans–Sackmann formula can be used for any Λ with an error less than 20% provided $(H/R)/\Lambda < 1$.

4.4. *Velocity fields and hydrodynamic interactions*

A final feature of these flows that we can investigate is the detailed velocity field. We first present the results of several simulations showing the structure of the surface velocity field and then we summarize in tabular form the manner in which the velocity decays in the far field. The section concludes with a remark about hydrodynamic interactions among surface-bound particles.

In figure 7 we show the variation of the radial component of the surface velocity field as a function of distance (r) for three different values of Λ and two sublayer depths, $H/R = 2000$ (solid curves) and $H/R = 10$ (long dashed curves). The shallow-sublayer limit $H/R = 1$ is illustrated in figure 8. There are several features worth

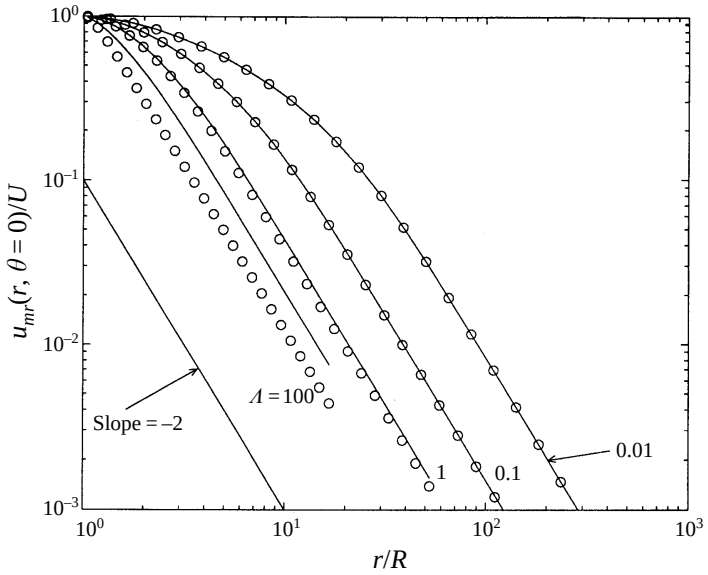

FIGURE 8. Radial velocity field as a function of the dimensionless radial distance for $H/R = 1$ and four values of $\Lambda = 100, 1, 0.1$ and 0.01; solid curves denote the numerical solution and the symbols are the velocity field calculated by Evans & Sackmann (1988) based on the thin-film model.

noting. First, as the sublayer thickness decreases the velocities decrease, as expected. Secondly, for the deep-sublayer limit, $H/R = 2000$, the velocity decays as $O(r^{-1})$ for $\Lambda > O(1)$, while for $\Lambda < O(1)$ there is a finite distance, predicted by the analytical arguments of Saffman (1976) (see Appendix B) to be $r = O(\ell_m = R\Lambda^{-1})$, where the velocities remain $O(1)$ and beyond which the velocities decay more rapidly as $O(r^{-1})$. Thirdly, in the shallow sublayer limit, the velocity clearly exhibits a decay rate $O(r^{-2})$ (figure 8), which is the decay rate expected owing to the influence of the nearby rigid boundary. Finally, we note that for the deep-sublayer limit, $H/R \gg 1$, an $O(r^{-2})$ decay rate is also expected but requires distances $r > O(H)$. This transition from a r^{-1} decay to a r^{-2} decay is shown in the inset of figure 7 for the case $\Lambda = 0.01$ and $H/R = 2000$. The $O(r^{-2})$ rate of decay is also to be expected eventually of the simulations with large Λ and $H/R = 2000$, but requires $r > O(H)$ and at these distances the velocities become very small indeed. The $O(r^{-2})$ rate of decay is predicted by the detailed velocity field calculated by Evans & Sackmann (1988) for thin sublayers, and may be thought of as arising from the two-dimensional surface pressure field that decays for translational motions as $O(r^{-1})$ (the pressure is harmonic), which requires that $|\boldsymbol{u}_m| = O(r^{-2})$ (see equation (22)); alternatively, the faster decay of the velocity field may be considered to be analogous to the similar decay in the three-dimensional viscous flow field of a point force tangent to a rigid boundary.

In figure 8, we compare the detailed velocity field calculated by Evans & Sackmann (1988) (the symbols) with the complete numerical solution for a sublayer depth $H/R = 1$ (solid curves). There is excellent agreement for $\Lambda \leqslant 0.1$, but the approximate solution is clearly less accurate for $\Lambda \geqslant 1$. In both cases, though, we observe that the influence of the nearby boundary leads to velocities that decay as $O(r^{-2})$. As a further illustration that for small Λ the Evans–Sackmann model has a wide applicability, we show in figure 7 the model's predictions (circles) of the velocity field for $\Lambda = 0.01$ and

$\Lambda \gg 1$ $H < R$	$u_m/U = O(R^2/r^2)$ for $r > R$	—	—
$\Lambda \gg 1$ $H > R$	$u_m/U = O(R/r)$ for $R < r < O(H)$	$u_m/U = O(RH/r^2)$ for $r > O(H)$	—
$\Lambda \ll 1$ $H > \ell_m > R$	$u_m/U = O(1)$ for $R < r < O(\ell_m)$	$u_m/U = O(\ell_m/r)$ for $O(\ell_m) < r < O(H)$	$u_m/U = O(\ell_m H/r^2)$ for $r > O(H)$
$\Lambda \ll 1$ $\ell_m > \ell_H > R$	$u_m/U = O(1)$ for $R < r < O(\ell_H)$	$u_m/U = O(\ell_H^2/r^2)$ for $r > O(\ell_H)$	—
$\Lambda \ll 1$ $\ell_m > R > \ell_H$	$u_m/U = O(R^2/r^2)$ for $r > R$	—	—

TABLE 3. Qualitative description of the decay of the surface velocity field as a function of distance from the object (logarithmic factors typically appear in the detailed expressions for the velocity). $\ell_m = \eta_m h/\eta$, $\ell_H = (\ell_m H)^{1/2}$, $\Lambda = R/\ell_m$.

$H/R = 10$. There is excellent agreement as 'thin' really corresponds to the requirement $H < \ell_m = R\Lambda^{-1}$, as has been previously indicated.

A qualitative description of the transitions in the velocity decay rate as a function of distance from the object for the different Λ regimes is summarized in table 3.

Influence on hydrodynamic interactions: With an understanding of the structure of the velocity field, it is natural to close this discussion by thinking about other problems for which the boundary influence may be important. Recently, Koch and Hammer and coworkers (Bussell *et al.* 1992, 1994; Dodd *et al.* 1995) examined hydrodynamic interactions among integral membrane proteins ($\Lambda \ll 1$) since hydrodynamic interactions should be expected to decrease diffusivities and all previous studies had neglected to account for this important effect.

The basic physical idea underlying the asymptotic analysis of the hydrodynamic interactions for a dilute system of proteins is clearly stated by these authors: on length scales comparable to the particle scale, or the interparticle spacing d provided $d < \ell_m$, the local flow is two-dimensional and velocity disturbances vary logarithmically. Beyond a distance ℓ_m, the surrounding fluid exerts stresses that cause the velocity disturbance to decay as $O(U\ell_m/r \ln(\Lambda^{-1}))$ (e.g. see the detailed analysis of Saffman's results given in Appendix B, and equations (C 1) and (C 3)). Calculations of the diffusivities as a function of the area fraction ϕ show that the variations from the infinite-dilution limit can be approximately summarized as (i) a decrease in the diffusivity that can be described by an increase in the effective shear viscosity of the membrane fluid from η_m to $\eta_m(1 + 2\phi)$, i.e. the Einstein viscosity in two dimensions, and (ii) an increase in the diffusivity owing to the velocity disturbances created by the other particles, which produces a change $O(\phi/\ln(\Lambda^{-1}))$ (Bussel *et al.* 1994). Term (i) is generally the most significant effect.

Thus, we may indicate the approximate effect of a nearby rigid planar substrate on the hydrodynamic interactions among integral membrane proteins in the dilute limit $\phi \ll 1$, with $H < \ell_m$, which is when the (small) area fraction of proteins and the finite depth are both significant. In particular, for free suspensions the logarithmic

divergences are now cut off on a length scale ℓ_H rather than ℓ_m. Therefore, we should expect the qualitative structure of the results of Bussel *et al.* (1994) to be applicable to the finite-depth case (with changes in the order-one coefficients) except that Λ^{-1} (their λ) should be replaced by ℓ_H/R. The numerically most important effect is still a decrease in the diffusivities due to the increased effective viscosity of the membrane (independent of H/R). Nevertheless, this physical argument shows that the influence of the disturbance flows produced by the other particles, which tend to increase the diffusivities, is diminished whenever $\ell_H < \ell_m$. Finally, these authors also studied fixed beds as models for plasma membranes (Dodd *et al.* 1995). We expect their results to hold for finite-depth sublayers provided the Brinkman screening length $R\phi^{-1/2}$ is smaller than ℓ_H.

5. Concluding remarks

In this paper we have described an exact solution for the translation of a circular cylinder, or disk, in a thin, flat surface film, which is a configuration that models the movement of membrane-trapped objects common in biology and physical chemistry. Numerical results for the drag on, or friction coefficient of, a steadily translating particle were presented for wide ranges of the dimensionless sublayer depth H/R and the viscosity ratio parameter Λ, i.e. $F = \eta R U \mathscr{F}(\Lambda, H/R)$ where $\mathscr{F}$ is determined numerically. The infinite- and thin-subphase limits previously analysed were recovered. The translational diffusion coefficient follows from $D_T = k_B T/\eta R \mathscr{F}$. Most importantly, the numerical results are well represented for all H/R by the combination of the Evans–Sackmann thin-sublayer formula (21) and the infinite-sublayer limit (for example, the equation of Hughes *et al.* (19) for $\Lambda \leqslant 0.6$; for $\Lambda > 0.6$ a numerical calculation is, in general, required).

We have further demonstrated that the detailed dynamical response is understandable in terms of the relative sizes of the four length scales $R, H, \ell_m = \eta_m h/\eta$ and $\ell_H = (\eta_m h H/\eta)^{1/2}$. The order of magnitude of the force on the membrane-bound object is controlled by the velocity gradients in the neighbourhood of the object, which may be affected by long-range fluid motions. For the common viscous monolayer or bilayer system, $\Lambda \ll 1$, there is a long length scale ℓ_m or ℓ_H beyond which the subphase resistance can no longer be neglected dynamically, and in these circumstances the local velocity gradient in the surface film near the translating particle varies as $U/R \ln(\ell/R)$, where $\ell = \min(\ell_m, \ell_H)$. We also derived an asymptotic result, equation (23), for the drag valid for finite-depth sublayers in the limit $\Lambda \ll 1$. Tables 1 and 2 summarize approximate scaling relationships for the order-of-magnitude of the force as H/R and Λ are varied and figures 4–6 illustrate the accuracy of the different analytical approximations. We closed by illustrating the form of the surface velocity fields and the qualitative modification to be expected when studying hydrodynamic interactions.

H.A.S. thanks A.A. and the Groupe de Physico-Chimie Théorique de l'ESPCI for their hospitality during a visit when this work was completed and H. M. McConnell for suggesting this problem. We thank A. Acrivos for a helpful conversation pointing out the manner in which equations (4*a*) and (4*b*) are related and D. A. Edwards for bringing several references to our attention. Also, we thank the referees for their thoughtful and insightful comments, including one referee who indicated the approach for developing the asymptotic solution for the finite layer described in Appendix B.

Appendix A. The limit $\Lambda \gg 1$, $H/R \gg 1$

In this Appendix we provide a brief derivation of the force and simplified flow field for the limit $\Lambda \gg 1$ and an infinitely deep fluid, $H/R \gg 1$. This limit was previously discussed by Hughes *et al.* (1981) though we feel it is easier to see the form of the result given the simplified presentation described in this paper of the solution to the dual integral equations.

We begin with (14). For $H/R \to \infty$ and $\Lambda \to \infty$, the leading-order approximation to the integral is

$$\sum_{m=0}^{\infty} a_m \int_0^{\infty} s^{-2-2\beta} J_{2m+1+\beta}(s) J_{2n+1+\beta}(s)\,\mathrm{d}s = \frac{\Lambda \delta_{0n}}{2^{\beta+1}\Gamma(\beta+2)}, \quad n = 0, 1, \ldots. \tag{A 1}$$

The integral is given in Gradshteyn & Ryzhik (1965, equation 6.574.2); it exists for $\beta > -1$, and so in this case choosing $\beta = -1/2$, we have

$$\int_0^{\infty} s^{-1} J_{2m+1/2}(s) J_{2n+1/2}(s)\,\mathrm{d}s = \delta_{nm}. \tag{A 2}$$

Therefore, equation (A 1) leads directly to

$$a_m = \frac{\sqrt{2}\Lambda}{\pi^{1/2}} \delta_{0m}. \tag{A 3}$$

The force on the translating disk is given by (16), and only involves a_0, and so we obtain

$$\frac{F}{4\pi\eta R U} = \frac{2}{\pi}. \tag{A 4}$$

As pointed out by Hughes *et al.* this result is greater than half the force acting on a rigid disk translating edgewise in a viscous fluid, for which one finds $4/3\pi$ instead of $2/\pi$. This difference (and indeed the increase) is a consequence of the flow being confined to move in planes $z =$ constant owing to the surface film, however thin, requiring the surface to remain flat.

Appendix B. An approximate force–velocity relation for $\Lambda \ll 1$ and a finite-depth subphase

Saffman (1976) developed an approximate solution for an unbounded subphase by considering the point-force limit of the governing equations with $\Lambda \ll 1$. This calculation, valid for $R \ll \ell_m \ll \ell_H \ll H$, is extended here to the finite-depth case with $R, H \ll \ell_H \ll \ell_m$. The calculation uses the idea of matched asymptotic expansions to describe both the region at large distances where the particle looks like a point force (the 'outer' region) as well as the region near the particle where the fluid motion is nearly that of a translating cylinder (the 'inner' region). We are indebted to a referee for suggesting this calculation.

We replace the particle by a point force $\boldsymbol{F} = F\boldsymbol{e}_x$ acting on the fluid and so first solve a modified form of (7)

$$-\nabla p_m + \eta_m \nabla^2 \boldsymbol{u}_m + \boldsymbol{f} + \frac{F\delta(r)}{2\pi r h}\boldsymbol{e}_x = \boldsymbol{0} \quad \text{and} \quad \nabla \cdot \boldsymbol{u}_m = 0, \tag{B 1}$$

which describes two-dimensional surface flow in the outer region driven by a point force parallel to the direction of particle motion.

Taking the curl of (B 1) eliminates the pressure, using the identities for cylindrical coordinates that

$$\nabla \wedge \left\{ \frac{\delta(r)}{r} \boldsymbol{e}_x \right\} = -\sin\theta\, (\boldsymbol{e}_r \wedge \boldsymbol{e}_\theta) \frac{\mathrm{d}}{\mathrm{d}r}\left(\frac{\delta(r)}{r}\right) \quad \text{and} \quad \int_0^\infty \frac{\mathrm{d}}{\mathrm{d}r}\left(\frac{\delta(r)}{r}\right) r J_1(kr)\,\mathrm{d}r = -k, \tag{B 2}$$

and then substituting the known form of the velocity fields for a finite-depth subphase, equations (3*a*) and (3*b*), leads to

$$UA(k)\sinh(kH) = \frac{F}{4\pi h \eta_m} \frac{1}{\left[k + (\eta/\eta_m h)\coth(kH)\right]}. \tag{B 3}$$

In the limit $H \to \infty$ we obtain Saffman's original result (note that there are differences of factors of 2 since Saffman accounts for fluid on both sides of the membrane).

The radial component of the corresponding outer flow then follows from (3*a*):

$$\begin{aligned} u_{mr}^{outer}(r,\theta) &= \frac{F\cos\theta}{4\pi h\eta_m} \int_0^\infty \frac{[J_0(kr) + J_2(kr)]}{k + (\eta/\eta_m h)\coth(kH)} \mathrm{d}k \\ &= \frac{F\cos\theta}{4\pi h\eta_m} \int_0^\infty \frac{[J_0(s) + J_2(s)]}{s + (\eta r/\eta_m h)\coth(sH/r)}\,\mathrm{d}s. \end{aligned} \tag{B 4}$$

The inner limit of the outer solution is obtained by letting $r \to 0$. In this limit the integral is dominated by the contribution from s near zero in (B 4). We may thus follow the spirit of Saffman's asymptotic analysis and add and subtract the integral of the denominator from 0 to 1. As such we may write

$$\lim_{r\to 0} \frac{4\pi h\eta_m}{F\cos\theta} u_{mr}^{outer}(r,\theta) = \lim_{r\to 0} \int_0^\infty \frac{[J_0(s) + J_2(s)]}{s + (\eta r/\eta_m h)\coth(sH/r)}\,\mathrm{d}s \tag{B 5a}$$

$$= \int_0^1 \frac{\mathrm{d}s}{s + (\eta r/\eta_m h)\coth(sH/r)} + \int_1^\infty \frac{J_0(s)}{s + (\eta r/\eta_m h)\coth(sH/r)}\,\mathrm{d}s \tag{B 5b}$$

$$+ \int_0^1 \frac{J_0(s) - 1}{s + (\eta r/\eta_m h)\coth(sH/r)}\,\mathrm{d}s + \int_0^\infty \frac{J_2(s)}{s + (\eta r/\eta_m h)\coth(sH/r)}\,\mathrm{d}s \tag{B 5c}$$

$$\approx \int_0^1 \frac{s\,\mathrm{d}s}{s^2 + (\eta r^2/\eta_m hH)} + \int_1^\infty \frac{J_0(s)}{s}\,\mathrm{d}s + \int_0^1 \frac{J_0(s) - 1}{s}\,\mathrm{d}s + \int_0^\infty \frac{J_2(s)}{s}\,\mathrm{d}s, \tag{B 5d}$$

where we have used the small-argument expansion of $\coth(t) \approx t^{-1}$ in the first term on the right-hand side of (B 5*d*) and neglected the coth term in all of the non-singular integrals. Evaluating each of the integrals yields (Abramowitz & Stegun 1972, equations 11.1.20 and 11.4.16)

$$u_{mr}^{outer}(r,\theta) \approx \frac{F\cos\theta}{4\pi h\eta_m} \left[-\frac{1}{2}\ln\left(\frac{\eta r^2}{\eta_m hH}\right) + \frac{1}{2} - \gamma + \ln 2 \right], \tag{B 6}$$

where $\gamma \approx 0.5772$ is Euler's constant. As a referee pointed out, this result can also be justified by a more systematic asymptotic analysis. In particular, the integral (B 5*a*) can be split at an intermediate length scale δ, where $r/\ell_H \ll \delta \ll 1$ with $\ell_H^2 = H\ell_m$, $\ell_m = \eta_m h/\eta$, and under the stated limits $H \ll \ell_H$. Then, as the denominator simplifies

to $s+(\eta r/\eta_m h)\coth(sH/r)\approx s$ for $s>\delta$, (B 5*a*) may be written

$$\lim_{r\to 0}\frac{4\pi h\eta_m}{F\cos\theta}u_{mr}^{outer}(r,\theta)=\lim_{r\to 0}\int_0^\infty\frac{[J_0(s)+J_2(s)]}{s+(\eta r/\eta_m h)\coth(sH/r)}\mathrm{d}s \tag{B 7a}$$

$$=\lim_{r\to 0}\int_0^\delta\frac{[J_0(s)+J_2(s)]}{s+(\eta r/\eta_m h)\coth(sH/r)}\mathrm{d}s+\int_\delta^\infty\frac{[J_0(s)+J_2(s)]}{s+(\eta r/\eta_m h)\coth(sH/r)}\mathrm{d}s \tag{B 7b}$$

$$\approx\int_0^\delta\frac{s}{s^2+r^2/\ell_H^2}\,\mathrm{d}s+\int_\delta^\infty\frac{[J_0(s)+J_2(s)]}{s}\mathrm{d}s \tag{B 7c}$$

$$\approx\frac{1}{2}\ln\left(\delta^2+\frac{r^2}{\ell_H^2}\right)-\frac{1}{2}\ln\left(\frac{r^2}{\ell_H^2}\right)+\int_\delta^\infty\frac{J_0(s)}{s}\mathrm{d}s+\int_0^\infty\frac{J_2(s)}{s}\mathrm{d}s \tag{B 7d}$$

which, in the limit $r/\ell_H\ll\delta\ll 1$, and using the tabulated integrals indicated above, then leads to (B 6), which is, of course, independent of δ.

On the other hand, the solution for the two-dimensional Stokes flow of a translating cylinder, which satisfies the no-slip boundary condition on the surface, gives (Batchelor 1967)

$$u_{mr}^{inner}(\bar r,\theta)=U\cos\theta\left[1+\beta\left(-\ln\bar r+\frac{1}{2}-\frac{1}{2\bar r^2}\right)\right], \tag{B 8}$$

where $\bar r=r/R$ and β is a constant to be determined by imposing the boundary condition at large distances. Matching the inner limit of the outer approximation (B 6) and the outer limit of the inner approximation (B 8) gives

$$\beta=\frac{F}{4\pi\eta_m hU}\quad\text{and}\quad U=\frac{F}{4\pi\eta_m h}\left(\ln\left(\frac{\Lambda R}{4H}\right)^{-1/2}-\gamma\right). \tag{B 9}$$

Thus, we see that the drag force exerted on the particle, accounting for a resistance from the finite-depth subphase, corresponds to $-\boldsymbol{F}$ in equation (B 1), and so

$$\boldsymbol{F}_{\text{finite depth}}=-\frac{4\pi\eta_m h\boldsymbol{U}}{\ln(\Lambda R/4H)^{-1/2}-\gamma}, \tag{B 10}$$

which was compared with the numerical results in figure 5.

Appendix C. The structure of the surface velocity field for $\Lambda\ll 1$

In this Appendix we justify the physical description utilized in the main body of the paper that for $\Lambda\ll 1$ and an infinitely deep subphase, corresponding to small objects in viscous fluid membranes, the typical velocity gradients in the membrane and measured near the particle occur on the length scale $R\ln(\Lambda^{-1})$. This result, though perhaps not fully appreciated, is demonstrated in a straightforward way using the analytical results given by Saffman (1976) and is similar to other two-dimensional, or 'nearly two-dimensional' flows involving cylindrically shaped objects. We could have presented these ideas using the point force solution for the finite-depth subphase, as developed in Appendix B, but since Saffman's calculation, and the Saffman–Delbrück model are familiar, it seemed appropriate to present a discussion based upon this simpler configuration.

We consider fluid motion in the surface film. At large distances from the translating object (i.e. in the 'outer' region), the flow may be characterized as that due to a point force, while the local flow in the neighbourhood of the object is basically the two-dimensional flow due to a translating cylinder. The point force solution to

the monolayer flow equation (B 1), including resistance offered by the unbounded subphase with no fluid above, yields a radial velocity field ($\bar{r} = r/R$)

$$u_{mr}^{outer}(\bar{r},\theta) = \frac{F\cos\theta}{4\pi h\eta_m}\int_0^\infty \frac{J_0(s)+J_2(s)}{(s+\Lambda\bar{r})}\,\mathrm{d}s, \tag{C 1}$$

which is the $H \to \infty$ limit of (B 4). We note that for large $\bar{r}$, i.e. $\bar{r}\Lambda > O(1)$, the integral is $O(\bar{r}^{-1})$ and so the far field has the usual unbounded Stokes flow decay rate.

Since the 'inner' limit of the outer equation (C 1) is (Saffman 1976)

$$\lim_{\bar{r}\to 0} u_{mr}^{outer} \approx \frac{F\cos\theta}{4\pi h\eta_m}\left[-\ln\bar{r} + \left(\ln(\Lambda^{-1}) + \tfrac{1}{2} - \gamma + \ln 2\right)\right] + \cdots, \tag{C 2}$$

then matching with the limit $\bar{r} \to \infty$ of the inner solution (equation B 8) shows

$$U = \frac{F}{4\pi\eta_m h}(\ln(2/\Lambda) - \gamma). \tag{C 3}$$

We thus observe that the local velocity field near the object has the form

$$u_{mr}^{inner}(\bar{r},\theta) = U\cos\theta\left[1 - \frac{1}{\left(\ln(2/\Lambda)-\gamma\right)}\left(\ln\bar{r} - \frac{1}{2} + \frac{1}{2\bar{r}^2}\right)\right], \tag{C 4a}$$

$$u_{m\theta}^{inner}(\bar{r},\theta) = U\sin\theta\left[-1 + \frac{1}{\left(\ln(2/\Lambda)-\gamma\right)}\left(\ln\bar{r} + \frac{1}{2} - \frac{1}{2\bar{r}^2}\right)\right]. \tag{C 4b}$$

The first term in each of these expressions corresponds to translation of the object and the second term shows that velocity gradients near the object are in fact $O(U/R\ln(\Lambda^{-1}))$.

It is worthwhile to close with an observation concerning four similar problems involving the translating cylinder geometry: (i) a long slender object with length $L \gg R$, where R is the cylinder radius, translating in an unbounded fluid at low Reynolds numbers, $\mathscr{R} = RU/\nu$, with $\mathscr{R} < R/L \ll 1$; (ii) a long slender object translating with $R/L < \mathscr{R} \ll 1$; (iii) a disk-shaped object translating in a viscous membrane with $\Lambda \ll 1$ (Saffman 1976); and (iv) translation with $\Lambda \ll 1$ in a viscous membrane adjacent to a sublayer of finite depth H. In each case the local two-dimensional Stokes flow corresponding to a cylinder translating parallel or perpendicular to its axis does not have a solution (Stokes's paradox for the case of translation perpendicular to the axis of the cylinder), but, beyond some distance ℓ, the flow problem is well posed and a solution exists. The basic mathematical structure is as described in this Appendix. Velocity gradients in the neighbourhood of the object do not occur on the length scale R but rather occur on the longer length scale $R\ln(\ell/R)$, where $\ell = L, R\mathscr{R}^{-1}$, $\ell_m = R\Lambda^{-1}$, or $\ell_H = R\left(R\Lambda/H\right)^{-1/2}$ for problems (i)–(iv), respectively. In the language of matched asymptotic expansions, working in a frame of reference with the object fixed and a uniform flow at large distances, it is necessary to pose an 'inner' expansion beginning with a term $O(\left[\ln(\ell/R) + \text{constant}\right]^{-1})$, while the outer expansion begins with a term $O(1)$; for example, see equation (C 4). Thus, the idea that the velocity gradients occur on a scale larger than the particle radius R, and involve a logarithmic factor of the ratio of two length scales, arises in several familiar circumstances.

REFERENCES

Abramowitz, M. & Stegun, I. A. 1972 *Handbook of Mathematical Functions.* Dover.

Batchelor, G. K. 1967 *An Introduction to Fluid Dynamics.* Cambridge University Press.

Brochard, F., Joanny, J. F., Andelman, D. 1987 In *Physics of Amphiphilic Layers* (ed. J. Meunier, D. Langevin & N. Boccara), pp. 13–19. Springer.

Bussell, S. J., Hammer, D. A. & Koch, D. L. 1994 The effect of hydrodynamic interactions on the tracer and gradient diffusion of integral membrane proteins in lipid bilayers. *J. Fluid Mech.* **258**, 167–190.

Bussell, S. J., Koch, D. L. & Hammer, D. A. 1992 The resistivity and mobility functions for a model of two equal-sized proteins in a lipid bilayer. *J. Fluid Mech.* **243**, 679–697.

Clegg, R. M. & Vaz, W. L. C. 1985 Translational diffusion of proteins and lipids in artificial lipid bilayer membranes. A comparison of experiment with theory. In *Progress in Protein-Lipid Interactions*, vol. 1, pp. 173–229. Elsevier.

Dodd, T. L., Hammer, D. A., Sangani, A. S., & Koch, D. L. 1995 Numerical simulations of the effect of hydrodynamic interactions on diffusivities of integral membrane proteins. *J. Fluid Mech.* **293**, 147–180.

Evans, E. & Sackmann, E. 1988 Translational and rotational drag coefficients for a disk moving in a liquid membrane associated with a rigid substrate. *J. Fluid Mech.* **194**, 553–561.

Gradshteyn, I. S. & Ryzhik, I. M. 1965 *Tables of Integrals, Series and Products.* Academic.

Hughes, B. D., Pailthorpe, B. A. & White, L. R. 1981 The translational and rotational drag on a cylinder moving in a membrane. *J. Fluid Mech.* **110**, 349–372.

Lucas, S. K. 1995 Evaluating infinite integrals involving products of Bessel functions of arbitrary order. *J. Comput. Appl. Maths* **64**, 269–282.

McConnell, H. M. 1991 Structures and transitions in lipid monolayers at the air–water interface. *Ann. Rev. Phys. Chem.* **42**, 171–195.

Merkel, R., Sackmann, E. & Evans, E. 1989 Molecular friction and epitactic coupling between monolayers in supported bilayers. *J. Phys. Paris* **50**, 1535-1555.

Peters, R. & Cherry, R. J. 1982 Lateral and rotational diffusion of bacteriorhodopsin in lipid bilayers: Experimental test of the Saffman–Delbrück equations. *Proc. Natl Acad. Sci.* **79**, 4317–4321.

Sackmann, E. 1996 Supported membranes: Scientific and practical applications. *Science* **271**, 43–48.

Saffman, P. G. 1976 Brownian motion in thin sheets of viscous fluid. *J. Fluid Mech.* **73**, 593–602.

Saffman, P. G. & Delbrück, M. 1975 Brownian motion in biological membranes. *Proc. Natl Acad. Sci.* **72**, 3111–3113.

Sneddon, I. N. 1966 *Mixed Boundary Value Problems in Potential Theory.* John Wiley & Sons.

Stone, H. A. & McConnell, H. M. 1994 Hydrodynamics of quantized shape transitions of lipid domains. *Proc. R. Soc. Lond.* A **448**, 97–111.

Stone, H. A. & McConnell, H. M. 1995 Lipid domain instabilities in monolayers overlying sub-layers of finite depth. *J. Phys. Chem.* **99**, 13505–13508.

Tanzosh, J. P. & Stone, H. A. 1995 Tranverse motion of a disk through a rotating viscous fluid. *J. Fluid Mech.* **301**, 295–324.

Tranter, C. J. 1966 *Integral Transforms in Mathematical Physics.* John Wiley & Sons.

Ungarish, M. & Vedensky, D. 1995 The motion of a rising disk in a rotating axially bounded fluid for large Taylor number. *J. Fluid Mech.* **291**, 1–32.

Vaz, W. L. C., Stümpel, J., Hallmann, D., Gambacorta, A. & De Rosa, M. 1987 Bounding fluid viscosity and translational diffusion in a fluid lipid bilayer. *Euro. Biophys. J.* **15** 111–115.